JOURNAL OF CATALYSIS 103, 366–384 (1987)

Studies of the Structure of Molybdenum Oxide and Sulfide Supported on Thin Films of Alumina

TERRY F. HAYDEN[1] AND J. A. DUMESIC[2]

Department of Chemical Engineering, University of Wisconsin, Madison, Wisconsin 53706

Received July 15, 1986; revised August 27, 1986

The morphology of monolayer quantities of molybdenum oxide and sulfide phases supported on thin films of nonporous alumina was studied by X-ray photoelectron spectroscopy and conventional and scanning transmission electron microscopy. Following oxidation at 770 K, a strong oxide–support interaction was observed, resulting in a highly dispersed molybdenum phase for loadings below ca. 5 Mo atoms nm^{-2}. The molybdenum oxide–support interaction was broken by sulfiding in H_2S/H_2 at ca. 770 K, with the formation of faceted single crystallites of MoS_2. The MoS_2 crystallites were present as hexagonally shaped slabs with one truncated edge and they were bonded with their high-energy edge planes to the alumina surface. The edge planes contacting the gas phase were the $(10\bar{1}0)$ set of planes, while the truncated edge bonded to the surface of alumina was the $(2\bar{1}\bar{1}0)$ plane. After 910 K sulfidation, the particles became larger, and many were oriented with their basal planes parallel to the support. Reoxidation at 770 K redispersed the crystallites due to spreading of molybdenum oxide over alumina. These results can be explained by the formation of Mo–O–Al linkages during oxidation and the breaking of these linkages during sulfiding. As these linkages that anchor the MoS_2 crystallites to the support are broken, the MoS_2 basal planes become oriented at angles close to 90° to the support surface. Upon more extensive sulfidation, the MoS_2 crystallites became oriented with their basal planes parallel to the support when the Mo–O–Al linkages at the edge plane are finally broken.

INTRODUCTION

Considerable effort has been directed toward characterizing the Mo-oxide and Mo-sulfide/γ-Al_2O_3 catalyst system because of its use in reactions such as hydrogenation (*1*), hydrodesulfurization (*2–5*), methanation (*6*), and water–gas shift (*7*). The activity of this system has been observed to be sensitive to the preparation conditions (*8*), and both the oxide and the sulfide forms of the catalyst have been thought to consist of highly dispersed molybdenum species bonded tightly to alumina (*3*). In the oxide form of the catalyst, a molybdenum oxide monolayer structure has been proposed to exist for low molybdenum loadings (*9, 10*), that has been undetectable from the alumina support in electron microscopy studies (*11*). Conversion to the sulfide form results in the formation of MoS_2 crystallites at sulfiding temperatures in excess of 670 K (*12*), and sintering occurs at higher temperatures (*13*).

For hydrodesulfurization (HDS) (*14, 15*) and hydrogenation (*15*), coordinately unsaturated molybdenum cations on the MoS_2 crystal edges are believed to be the active sites. In studies that involved cobalt-promoted Mo/Al_2O_3 catalysts, a Type II structure was formed at high sulfiding temperatures that had a higher specific HDS activity than a Type I structure that was formed at low sulfiding temperatures (*16, 17*). The difference in activity between the two structures was believed to be dependent on the MoS_2 structural interaction with the support. In addition, the MoS_2 morphology itself may be important in determining catalytic activity, because corner and edge plane sites along MoS_2 edges are believed to differ in catalytic activity (*8, 18*).

[1] Present address: IBM Systems Technology Division, 11400 Burnet Rd., 34D/045, Austin, Tex. 78758.

[2] To whom correspondence should be addressed.

0021-9517/87 $3.00

In this work, the microstructure of Mo-oxide/γ-Al_2O_3 and Mo-sulfide/γ-Al_2O_3 thin film, model catalysts was studied to elucidate the interactions between Mo-species and alumina. Low-surface-area model catalysts, which consisted of thin polycrystalline films of γ-Al_2O_3 upon which molybdenum was deposited, were chosen over conventional catalysts of high surface area because of the advantages in characterization. In the oxide form of the catalyst, the highly dispersed Mo-oxide overlayer present on alumina was analyzed by X-ray photoelectron spectroscopy (XPS). In particular, use of the flat film support enabled surface compositions to be obtained by X-ray photoelectron spectroscopy without the complexities caused by the pore structure associated with the conventional catalysts. The MoS_2 particles arising from the sulfidation treatments were imaged *ex situ* with both conventional and scanning transmission electron microscopy (CTEM and STEM). Use of thin film alumina instead of high-surface-area alumina reduced the interference from contrast features of the support, thereby allowing detailed features in the bright field images associated with molybdenum. In the STEM, microchemical analysis of individual particles was accomplished with energy-dispersive X-ray analysis (EDX). Particle crystal structures and the orientation of MoS_2 edge planes with respect to the support were determined with microdiffraction analysis.

EXPERIMENTAL

Specimen Preparation Methods

Model MoO_3/γ-Al_2O_3 catalysts were prepared that consisted of thin layers of molybdenum oxide deposited on thin (ca. 5-nm-thick) films of γ-Al_2O_3, as described in detail elsewhere (*19*). In short, thin alumina support films were formed by anodization of 0.025-mm-thick Al foils (Alfa). A nonporous amorphous Al_2O_3 film was grown on the foil by anodization in a 3% (w/w) aqueous tartaric acid electrolyte that had been previously adjusted to pH 7.0 with NH_4OH. To achieve regular buildup of the film, the voltage was first increased at a constant current density of 1 mA cm^{-2} until a constant voltage was reached, and then the current was allowed to exponentially decay to zero at constant voltage (*20–26*). The voltage has been shown to be proportionally related to the thickness of the oxide layer with a value of 1.34 nm V^{-1} (*27*). Next, each foil was scribed on one surface and immersed in a bromine–methanol solution (Br_2 : MeOH : H_2O, volume ratio 5 : 94 : 1) (*26*). The solution dissolved the metal in small holes (ca. 1–10 μm diameter) at places where the alumina backing had been damaged by the scribing, leaving the remainder of the Al foil backing intact. After washing and drying, the amorphous alumina layer was partly crystallized into γ-alumina by annealing the foil at 870 K for ca. 90 ksec in flowing oxygen.

Molybdenum oxide overlayers (MoO_3 powder, Alfa, 99.998% metals purity) were deposited onto the alumina film by vacuum evaporation from a resistively heated, alumina-covered molybdenum boat (R. D. Mathis, ME4-AO) at ca. 10^{-4} Pa. A calcined sample, MoO_3/γ-Al_2O_3, was formed by oxidation of the specimen at 770 K for 70 ksec in flowing O_2. A sulfided sample, MoS_2/γ-Al_2O_3, was prepared by treating the calcined catalyst at 670 or 770 K for 180 ksec in 6% H_2S/H_2 (Matheson, used as received). Some of these sulfided samples were also reoxidized at 770 K for 100 ksec in O_2.

XPS Measurements

The XPS measurements were carried out at 10^{-7} Pa with a Physical Electronics, Model 548, ESCA/Auger electron spectrometer equipped with a Mg anode, operating at 15 kV and 20 mA. High-resolution scans (over a 20-eV range) were performed of the Mo(3*d*), Al(2*p*), O(1*s*), and C(1*s*) regions at typically 25-eV pass energy. Peak positions were reported relative to a 74.2-eV reference energy of Al(2*p*) in Al_2O_3. The

high-resolution spectra were corrected for source and machine broadening with a deconvolution computer algorithm, based on the van Cittert method (*19, 28–34*). The ratios between the peak areas were calculated to give the experimental signal ratio, I_{Mo}/I_{Al}.

The expression for the intensity ratio between elements for a sample consisting of a uniform layer of thickness, t, on top of a semi-infinite substrate (e.g., Mo and Al in MoO_3/Al_2O_3) is (*35*)

$$\frac{I_{Mo}}{I_{Al}} = \frac{n_{Mo}}{n_{Al}} \frac{S_{Mo}}{S_{Al}} \frac{1 - \exp \frac{-t/\sin\theta}{\lambda(E_{k,Mo(3d_{5/2})})}}{\exp \frac{-t/\sin\theta}{\lambda(E_{k,Al(2p)})}},$$

where n_i is the atomic density of i in the compound, S_i is the relative atomic sensitivity factor, $\lambda(E_{k,x})$ is the mean free path for an electron with kinetic energy, $E_{k,x}$, for the transition, x, and θ is the angle between the detector and the surface of the specimen.

The reciprocal of the surface density for one full monolayer of coverage should be equal to about 0.20 nm^2 Mo $atom^{-1}$, obtained in independent experiments by other workers (e.g., (*36*)). The thickness of one monolayer should be about 0.255 nm based on the above surface density divided by the bulk density of MoO_3. Combining this result with the value of the thickness, t, in the previous equation leads to an approximation of the average number of monolayers, n_{ML}, of MoO_3 covering the support:

$$n_{ML} = t/(0.255 \text{ nm}).$$

CTEM and STEM Measurements

Studies employing CTEM were performed on 3-mm specimens, punched from the foils, using a JEOL 100B electron microscope operating at 100 kV. The STEM measurements were made using a Vacuum Generators HB501 microscope capable of bright field, annular dark field (ADF), microdiffraction, and energy-dispersive X-ray analysis. During EDX and microdiffraction analyses, the electron probe was focused on the area to be analyzed and then the sampling area was either set by the width of the electron probe itself (ca. 1 nm) or was set to be a 10 × 10-nm area for analyzing particles having sizes greater than 5 nm.

For EDX analysis, energy spectra were collected for 100 sec for the Al($K\alpha$) and Mo($L\alpha$) transitions at 1.49 and 2.29 keV, respectively. For microdiffraction analysis, the diffraction pattern was viewed on a fluorescent screen.

RESULTS

Al_2O_3 Support

X-ray photoelectron spectra of the alumina blank showed O(1*s*) and Al(2*p*) peak positions consistent with literature values for γ-Al_2O_3, and the O : Al intensity ratios were also consistent with the 1.5 stoichiometry of alumina. Electron micrographs revealed a broken and folded alumina overlayer attached to the thick aluminum backing. Only the thinnest and most transparent regions of the support film were studied. Selected-area diffraction patterns of these thin regions of alumina showed the presence of a few characteristic spots of *fcc* γ-Al_2O_3 in a ring pattern, indicating that the support was at least partly polycrystalline and also probably partly amorphous.

XPS Studies of MoO_3/Al_2O_3 Samples

Model catalysts of three different Mo loadings were prepared, as summarized in Table 1. Values reported for the MoO_3 thicknesses should be considered only relative to each other because the calculations assume a uniform thickness and the XPS technique has a photoelectron depth penetration greater than the thickness values listed in the table. Two of the samples (high and intermediate loadings) had Mo loadings greater than 1 monolayer, and the low-loading sample had less than one monolayer loading. The three samples used in this

TABLE 1

XPS Results for $MoO_3/Al_2O_3/Al$ Samples

Specimen loading	Specimen treatment	Peak	Peak position[a] (eV)	Area ratio with Al(2p) after deconvolution	MoO_3 thickness, n_{ML}[b]
High	After MoO_3 evaporation	Mo($3d_{5/2}$)	231.8	7.875	6.7
		O(1s)	—	—	
		Al(2p)	74.2	1.	
	After calcination	Mo($3d_{5/2}$)	231.8	0.7099	0.92
		O(1s)	530.6	8.452	
		Al(2p)	74.2	1.	
Intermediate	After evaporation	Mo($3d_{5/2}$)	231.7	2.167	2.5
		O(1s)	—	—	
		Al(2p)	74.2	1.	
Low	After evaporation	Mo($3d_{5/2}$)	231.6	0.06222	0.088
		O(1s)	—	—	
		Al(2p)	74.2	1.	
	After calcination	Mo($3d_{5/2}$)	231.5	0.1139	0.16
		O(1s)	530.3	7.346	
		Al(2p)	74.2	1.	

[a] Peak positions are referenced to the Al(2p) peak position of 74.2 eV.
[b] Details of the calculations are included in Ref. (*19*).

study span MoO_3 loadings of 0.17 to 6.7 monolayers as compared to industrial catalysts which have typical loadings of 1 monolayer.

Peak positions of Mo($3d_{5/2}$) and O(1s) photoelectrons agreed within error (taking into account the 0.8 eV width of the Mg $K\alpha$ source) to the literature values of 232.5 and 531.0 eV, respectively (*19, 37, 38*). The XPS signal ratios, I_{Mo}/I_{Al}, for all the model catalysts before and after calcination were consistent with the MoO_3-overlayer structures depicted in Fig. 1. Samples with loadings higher than one monolayer showed a decrease in the Mo : Al ratio upon calcination; however, samples with loadings less than one monolayer showed an increase in the Mo : Al ratio, which indicated an increase in Mo dispersion.

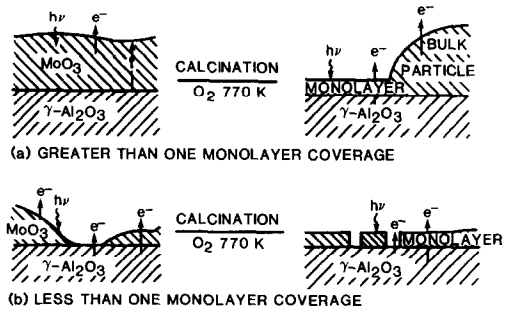

FIG. 1. Schematic of the structure of MoO_3 overlayers in the model catalyst before and after calcination.

Electron Microscopy Studies of Mo/Al_2O_3 Samples

TEM studies of high-loading specimen-calcined state. The bright field image after calcination of the model catalyst with 6.7 monolayers MoO_3 showed the presence of particles on a thin, featureless alumina support. The particle sizes were predominantly in the 50- to 100-nm range. EDX analysis (in STEM) showed that both the particles and the surrounding regions of the alumina contained Mo. The selected-area diffrac-

tion pattern showed the characteristic ring patterns of γ-Al_2O_3 and orthorhombic MoO_3, thus identifying the particles as MoO_3.

TEM studies of intermediate-loading specimen-calcined state. Electron micrographs after calcination of the model catalyst with 2.5 monolayers of MoO_3 showed the presence of particles, but with a much lower number density than was observed for the high-loading sample. Also, the particles were surrounded by large areas that appeared to be featureless, as the alumina blank. The particles possessed various sizes and shapes, ranging from 10-nm circular particles to irregularly shaped particles with dimensions as large as 250 nm.

Selected-area diffraction patterns showed the characteristic patterns of polycrystalline γ-Al_2O_3 and orthorhombic MoO_3, with no evidence for $Al_2(MoO_4)_3$. Energy-dispersive X-ray analysis was also performed on particles of various sizes and on the featureless background regions of the model catalyst with Mo loading of 2.5 monolayers (see Table 2). Both the featureless background and the particles contained significant amounts of Mo. This suggests that Mo was present in a highly dispersed form on alumina and as particles.

TEM studies of intermediate-loading specimen-sulfided state. Electron micrographs of the specimen with intermediate loading (2.5 monolayers MoO_3) showed several changes in overlayer morphology after mild sulfiding (6% H_2S/H_2 at 670 K, 180 ksec) as compared to after calcination. The most significant changes created by this treatment were an increased graininess in the "featureless" background due to nanometer-sized features in the background, an increased contrast in the large MoO_3 crystallites indicating that they were beginning to break-up, and the formation of a number of small, dark-contrast, elongated particles (smaller than 10 nm) appearing mostly near the larger particles that had been identified as MoO_3 in the calcined catalyst. In all of the regions examined this graininess was found to be uniform throughout the background.

TABLE 2

Microchemical EDX Analysis of Calcined $MoO_3/Al_2O_3/Al$ (Intermediate-Loading Catalyst)

Region	Feature	$\frac{Mo(L_\alpha)\ Area^a}{Al(K_\alpha)\ Area}$
I	Large particle (50–80 nm)	0.283
	Small particle (15–20 nm)	0.143
	Featureless background	0.111
II	15-nm particle	0.138
	15-nm particle	0.123
	15-nm particle	0.153
	Featureless background	0.116
III	Featureless background	0.110
	Featureless background	0.102
	Average: Featureless background	0.110 ± 0.005

[a] Raw data appear in Ref. (*19*).

This sample was further sulfided at 670 K for 180 ksec and at 770 K for 360 ksec, and it was examined by CTEM after each treatment. In general, higher sulfiding temperature caused an increase in the number of larger-sized, dark-contrast, elongated particles. Sulfiding at a higher temperature (770 K) resulted in a further break-up of the large MoO_3 particles into a collection of smaller elongated ones.

TEM studies of low-loading specimen-calcined state. Unlike the previous two specimens, which had MoO_3 loadings greater than one monolayer, electron micrographs of the specimen with low loading after calcination (0.17 monolayers MoO_3) (see Fig. 2) were similar to the Al_2O_3 blank and did not show the presence of particles. Figure 2 shows an essentially featureless sample that has been broken, and partly split in the middle, and the presence of low-contrast, round features of 5–10 nm (or smaller) that were uniformly distributed on the film. These features were also present in other regions of this specimen. Annular dark field (ADF) imaging of another region clearly highlighted these features from the background. Because ADF has a higher sensitivity to elements of high atomic num-

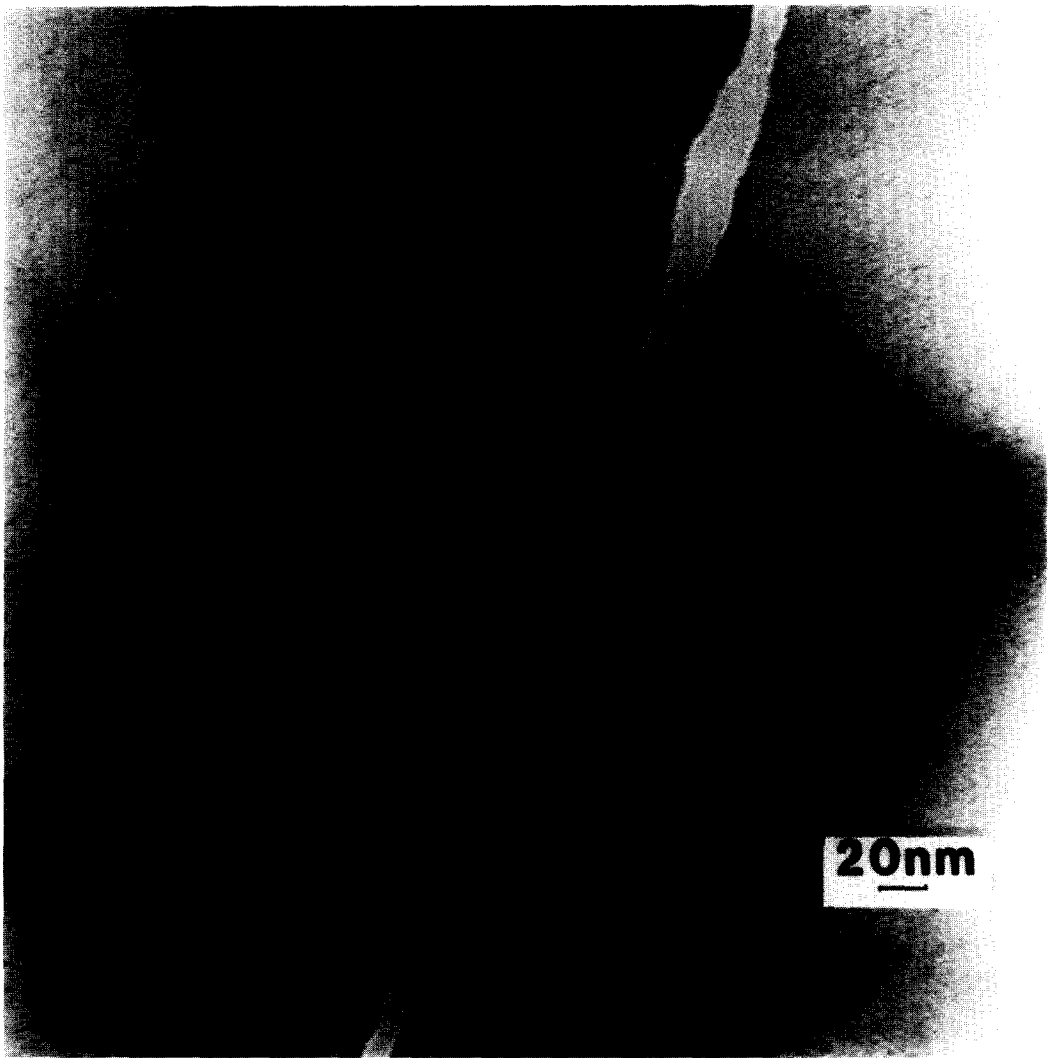

FIG. 2. High magnification CTEM micrograph of $MoO_3/Al_2O_3/Al$ with low loading after calcination: O_2, 770 K, 70 ksec.

ber (the signal is proportional to $Z^{3/2}$), these features could be due to Mo species, although possibly they could be crystalline regions of γ-Al_2O_3 because the ADF image is also sensitive to these features (*39*). Selected-area diffraction of thin regions of these specimens gave only an amorphous pattern with no γ-Al_2O_3, orthorhombic MoO_3, or $Al_2(MoO_4)_3$ spots or rings being observed.

TEM Studies of low-loading specimen-sulfided state. The calcined specimen with 0.17 monolayers of MoO_3 was subsequently sulfided in 6% H_2S/H_2 for 180 ksec and then for another 180 ksec (total of 360 ksec) at 670 K; it was next treated for 180 ksec at 770 K. Observation of the fluorescent screen in the CTEM revealed that the former treatments at 670 K produced no readily apparent differences as compared with the micrographs of the specimen in the calcined state. However, sulfiding at 770 K produced major changes in the bright field images with the formation of both round

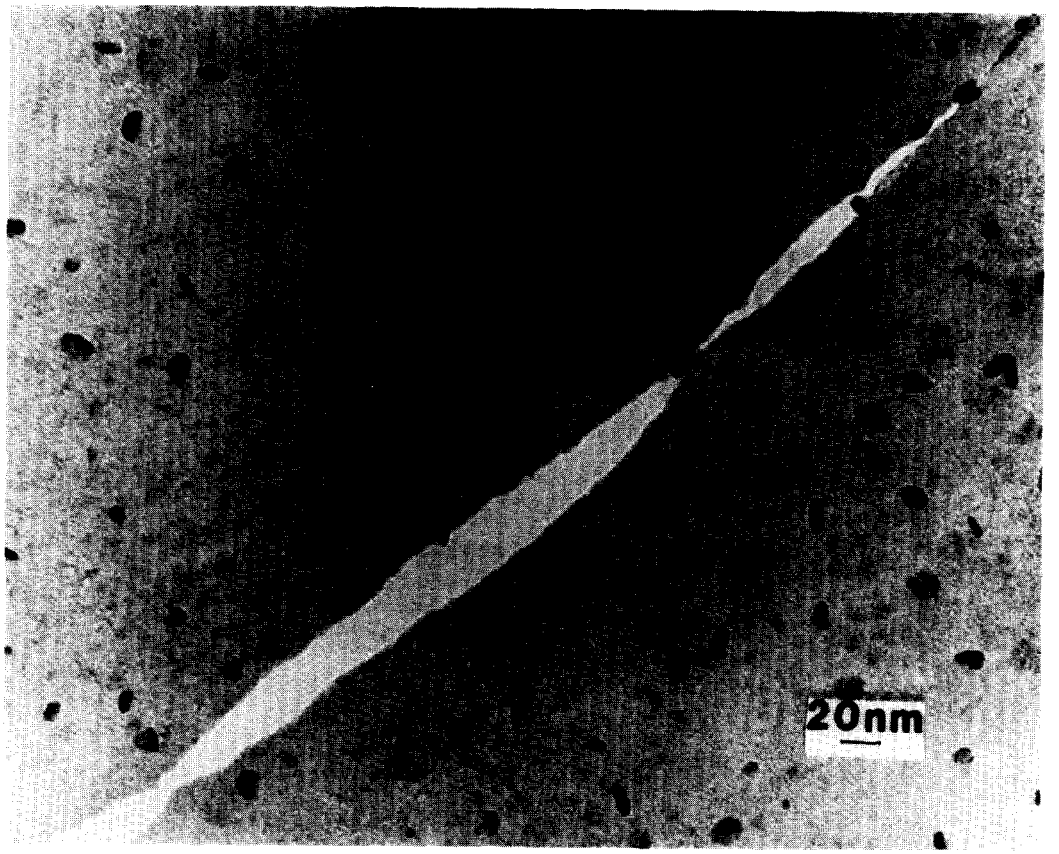

FIG. 3. High magnification CTEM micrograph of $MoO_3/Al_2O_3/Al$ with low loading after sulfiding, 6% H_2S/H_2, 770 K, 180 ksec, which showed the formation of particles as compared with the same region in the calcined state (see Fig. 4).

and elongated particles. Figures 3 and 4 are bright field CTEM micrographs of two sets of regions of the low-loading sample. It is important to note that sulfiding an alumina blank at both 670 and 770 K did not produce particles.

Electron microdiffraction analyses were performed on a number of round and elongated particles. All particles analyzed were identified as hexagonal MoS_2 single crystals (*40*); however, they were present on the sample in different orientations with respect to the electron probe direction (see Table 3).

Hexagonal MoS_2 ($P6_3/mmc$) is the most common form of molybdenum disulfide; it is a layer structure with parallel planes, the basal planes, extending along the *a* and *b*

TABLE 3

Summary of Microdiffraction Results

Electron beam direction (as referenced to the MoS_2 crystal axes)[a]	Angle of orientation between the particles's *c* axis and the electron beam direction[b]	Minor × major axis of particle (nm × nm)	Minor axis/major axis
$(\bar{1}10)$	90°	4 × 10	0.4
$(\bar{1}51)$	55°	6 × 15	0.4
$(\bar{2}31)$	48°	7 × 10	0.7
$(0\bar{3}1)$	38°	20 × 20	1.0
$(\bar{2}11)$	34°	20 × 20	1.0
$(\bar{1}31)$	34°	5 × 5	1.0
$(0\bar{2}1)$	27°	8 × 8	1.0
$(0\bar{2}1)$	27°	25 × 25	1.0
$(\bar{1}\bar{2}1)$	24°	18 × 18	1.0
$(\bar{1}\bar{2}1)$	24°	7 × 9	0.8
$(\bar{1}\bar{2}1)$	24°	35 × 35	1.0
$(0\bar{1}1)$	14°	10 × 15	0.7

[a] Pattern indexing is described in Ref. (*19*).

[b] 90° indicates that the electron probe is directly incident on the edge plane of the particle.

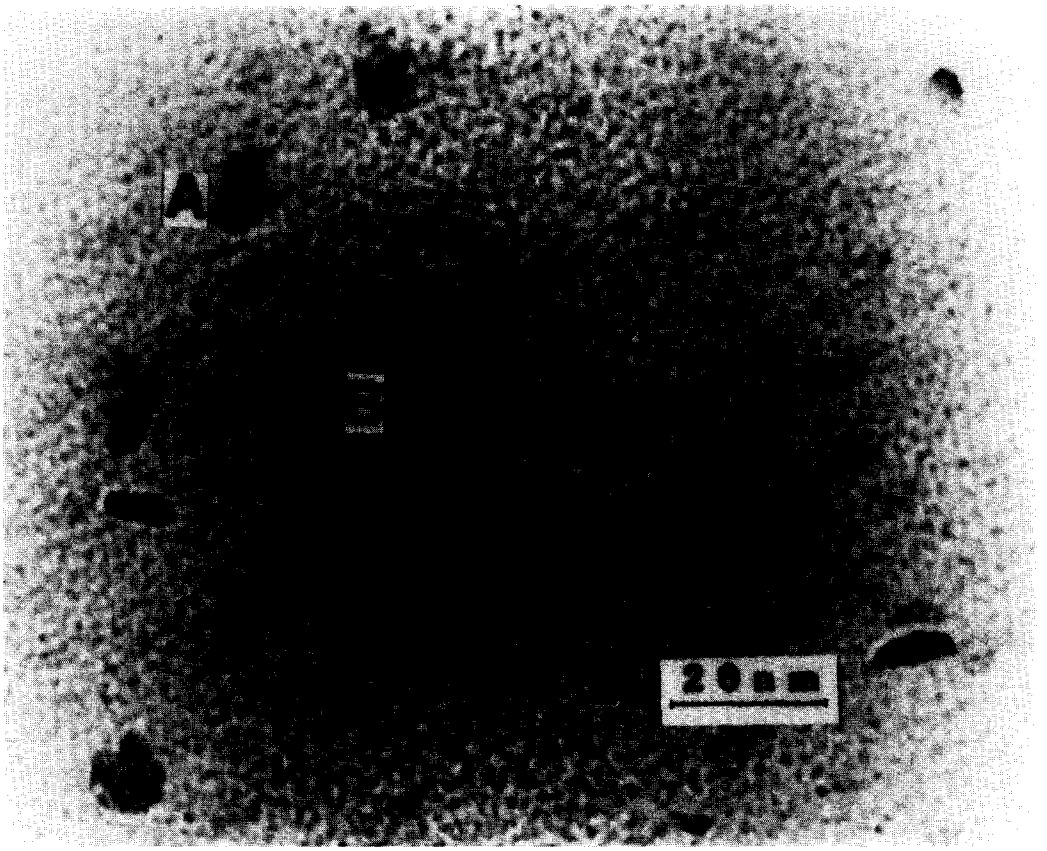

FIG. 4. Very high magnification CTEM micrograph of $MoO_3/Al_2O_3/Al$ with low loading after sulfiding: 6% H_2S/H_2, 770 K, 180 ksec.

axes and stacked along the c axis. The strong bonding along two dimensions and the weak bonding along the c-direction in MoS_2 lead to two major types of exposed surface planes for MoS_2 crystallites: the basal plane surface, (0002), and the two most stable edge plane surfaces, $(1\bar{0}10)$ (see Fig. 5a) and $(2\bar{1}\bar{1}0)$ (see Fig. 5b). The MoS_2 basal plane is more stable than the edge plane because the basal sulfur atoms each have three bonds to molybdenum cations and thus have completely filled $3s^23p^6$ octets, whereas the edge plane sulfur atoms have fewer than three bonds to molybdenum and are coordinately unsaturated. It should be noted that the depicted edge surface structures do not take into account charge neutrality and relaxation effects, which have been discussed by other workers (*41–43*).

Bonding of MoS_2 to Al_2O_3 supports has usually been visualized in terms of the MoS_2 layers lying parallel to the support surface with the basal plane interacting with the alumina surface atoms (e.g., (*2*)). However, considering that the high-energy edge planes may be stabilized by bonding into alumina, it is also possible to have MoS_2 crystallites bonded edgewise to the support with the c axis parallel to the surface. The two types of orientations of MoS_2 crystallites with the support are visualized in Fig. 6.

In addition to identifying the particles produced by sulfiding as MoS_2, microdiffraction analyses of the particles gave insight into the orientation and shapes of supported MoS_2 species. The microdiffraction results are compared in Table 3 to the mea-

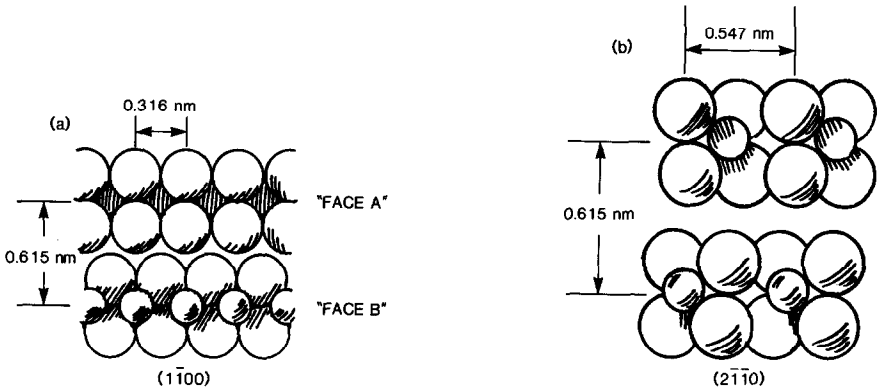

FIG. 5. Schematic drawings of edge planes of MoS_2. (a) (1$\bar{1}$00) plane; (b) (2$\bar{1}\bar{1}$0) plane.

sured dimensions of the particles analyzed in bright field STEM images in terms of a minor and major dimension of the elongated particles. The particles are ranked in this table in decreasing angles of orientation between the MoS_2 *c* axis and electron beam direction. Indeed, the two most highly elongated particles in the study had microdiffraction patterns (Fig. 7) that indicated that they were oriented with their basal planes nearly parallel to the electron beam (*c* axis at angles of 90 and 55°, respectively). The particle associated with Fig. 7a was particularly important; the *c* axis in reciprocal space was perpendicular to the electron beam and coincided with the direction of the minor axis determined in the bright field image. This indicated that the MoS_2 crystallite dimension along its basal plane was much larger than its dimension along the *c* axis. The 4-nm minor dimension for this particle corresponded, therefore, to a stacking of ca. 6–7 MoS_2 layers for this particle.

Comparison of the bright field micrographs in Figs. 2 and 3 shows the formation of the MoS_2 particles in the same region during sulfiding. Different particles in the sulfided specimen have different contrasts with respect to the alumina film, with the darkest particles generally being the most elongated. This is probably because these particles are thicker in the direction parallel to the electron beam. Although some of the rounded particles appear to be dark, these exceptions were most likely due to diffraction effects, the particles being oriented close to a Bragg angle. Besides the presence of elongated particles of different shapes and contrasts, the high magnification micrograph of Fig. 4 also shows the presence of a finer structure in the film between the larger elongated particles that is composed of dark dots smaller than about 2 nm. These features are similar to that observed in the MoS_2/Al_2O_3 specimen with intermediate loading after sulfiding but there is a lower density of these structures in the field of view. Because the density of this structure appears to increase with Mo loading, the structure is most likely attributable to small MoS_2 particles. The presence of

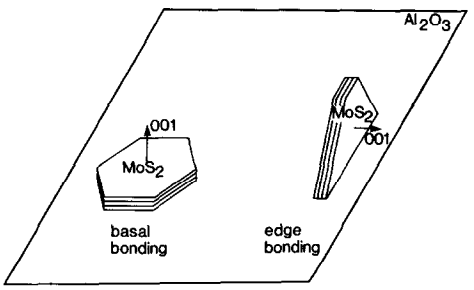

FIG. 6. Basal and edge bonding of MoS_2 crystallites to Al_2O_3. The individual layers or slabs of MoS_2 are depicted in the diagram.

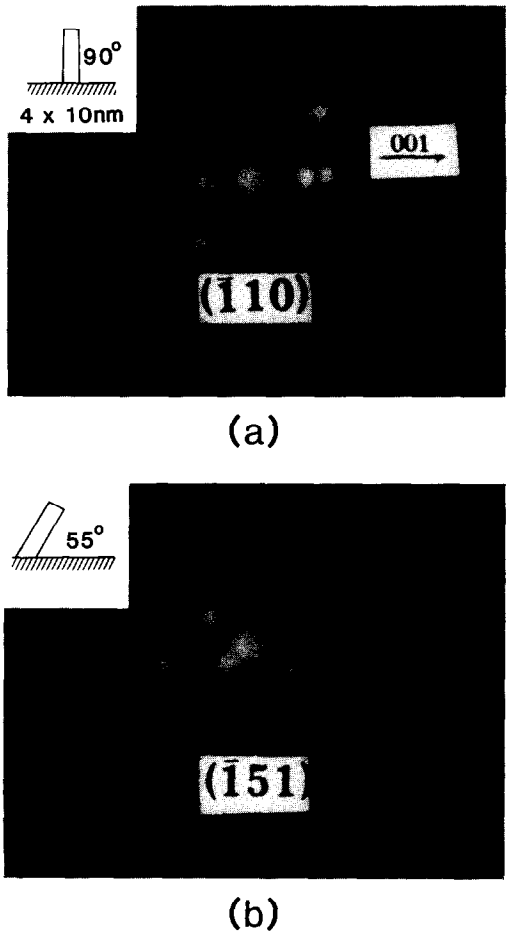

FIG. 7. Microdiffraction patterns of individual MoS_2 particles. (a) Microdiffraction pattern of a 4-nm × 10-nm particle that was indexed as the $\bar{1}10$ zone axis of hexagonal MoS_2. The 001 direction corresponds to the 4-nm dimension of the particle. (b) Microdiffraction of a 6-nm × 15-nm particle that was indexed as the $\bar{1}51$ zone axis of hexagonal MoS_2.

dark lines in Fig. 4 is apparent on many of the MoS_2 particles, and the orientation of these lines is along the major dimension of the particle. The highly elongated particle in the upper left of this figure (see feature at A) illustrates this phenomenon. The width of the lines in this particle is about 1 nm, which is the approximate width of one or two MoS_2 layers. Another feature which is present in these micrographs is represented by the particle in the lower right corner of Fig. 4 (see feature at B). Like many rounded particles, this particle appears to be more distinct on one side of the minor axis, with the opposite side being more diffuse. In addition, the more distinct edge appears to be more rounded than the more diffuse edge. It may be suggested that the more diffuse edge of the particle is bonded to the alumina support; and, the opposite edge is oriented away from the support, allowing it to adopt a well-defined edge.

Another model catalyst with a MoO_3 loading less than one monolayer was sulfided in 6% H_2S/H_2 at 840 K for 180 ksec and at 910 K for 100 ksec. In addition to a large number of small particles that were also observed after sulfiding at 770 K, the CTEM micrographs reveal a larger average particle size and the presence of either highly elongated particles or less elongated, faceted particles (see Fig. 8). From the aforementioned microdiffraction results, the highly elongated particles (see feature at a in Fig. 8) can be identified as MoS_2 crystallites bonded with their edge planes to and oriented close to 90° with the alumina surface. The faceted particles (see feature at b in Fig. 8) were similar to some of the particles observed after lower temperature sulfiding (770 K), in that one edge is diffuse and straight compared with the other edges. The faceted particles have sides that are consistently at 120° with respect to each other, except for the diffuse edge that appears to truncate the hexagon, which in most cases is oriented at 90° angles with respect to its adjacent edges. The general hexagonal shape indicates that the particles were MoS_2 single crystals that had undergone growth of a certain stable, six-member set of surface planes. The two most stable sets of edge plane surfaces are $(10\bar{1}0)$ and $(2\bar{1}\bar{1}0)$, as mentioned earlier. Both sets of planes form perfect hexagons with angles of $60n°$ (where n is an integer) among themselves, and the angles between the $(10\bar{1}0)$ and $(2\bar{1}\bar{1}0)$ sets are $[30 + 60n]°$. The surface energy of the latter plane, $(2\bar{1}\bar{1}0)$, can be estimated to be 15% higher than that of the former plane, $(10\bar{1}0)$ (*19*).

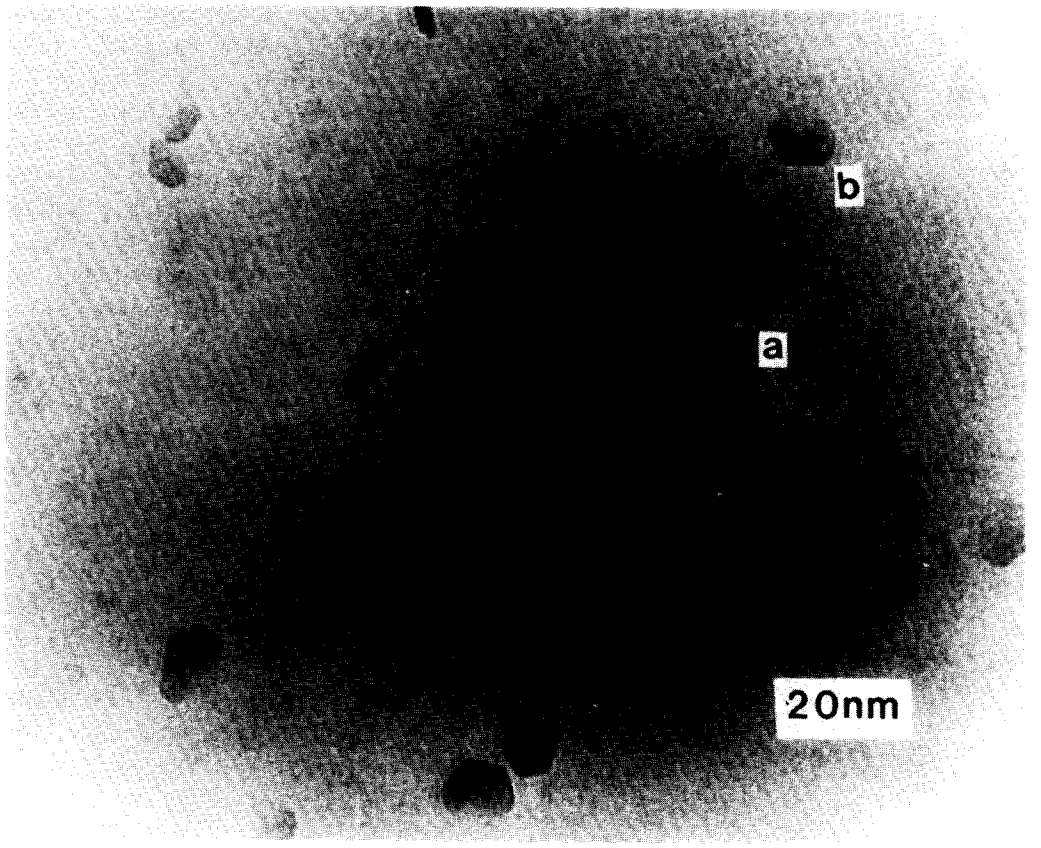

FIG. 8. High magnification CTEM micrograph of $MoO_3/Al_2O_3/Al$ after sulfiding: 6% H_2S/H_2, 910 K.

In contrast to the edges that formed the sides of the hexagon, the truncated edge indicates that there was an obstacle to growth. This is most likely attributable to this truncated edge being bonded (or having been bonded) to the alumina support surface. Its diffuse nature as compared with other darker edges may also show that this truncated edge is thinner than the other edges. The 90° angle between the truncated edge and the adjacent edges also indicates that the edge plane of bonding between MoS_2 and Al_2O_3 is of a different six-member set of planes than the set of edge planes contacting the gas phase. From the above considerations, the truncated edge would be the $(\bar{2}110)$ plane, a member of the $(2\bar{1}\bar{1}0)$ set of planes.

Identification of the $(2\bar{1}\bar{1}0)$ set as forming the truncated edge and $(10\bar{1}0)$ as forming the other edges is consistent with geometrical bonding considerations of MoS_2 with the Al_2O_3 surface. The most stable surface plane of face-centered cubic γ-Al_2O_3 is believed to be the (110) plane (*2, 44*), which has oxygen anions that are closely packed in rows (see the alumina surface portion of Fig. 9). In comparison, the molybdenum in the MoS_2 $(2\bar{1}\bar{1}0)$ surface are also arranged in rows (which make up the slabs of MoS_2 in three dimensions). The Mo–Mo distance within the rows (or slabs) is only 2% less than twice the O–O spacing within the oxygen rows of Al_2O_3 (110). In addition, the Mo–Mo distance between alternate rows (or slabs) in MoS_2 $(2\bar{1}\bar{1}0)$ is only 4% greater than the O–O spacing between every third row of Al_2O_3 (110). In one possible bonding scheme shown in Fig. 9, every molybdenum in alternate MoS_2 slabs is bonded

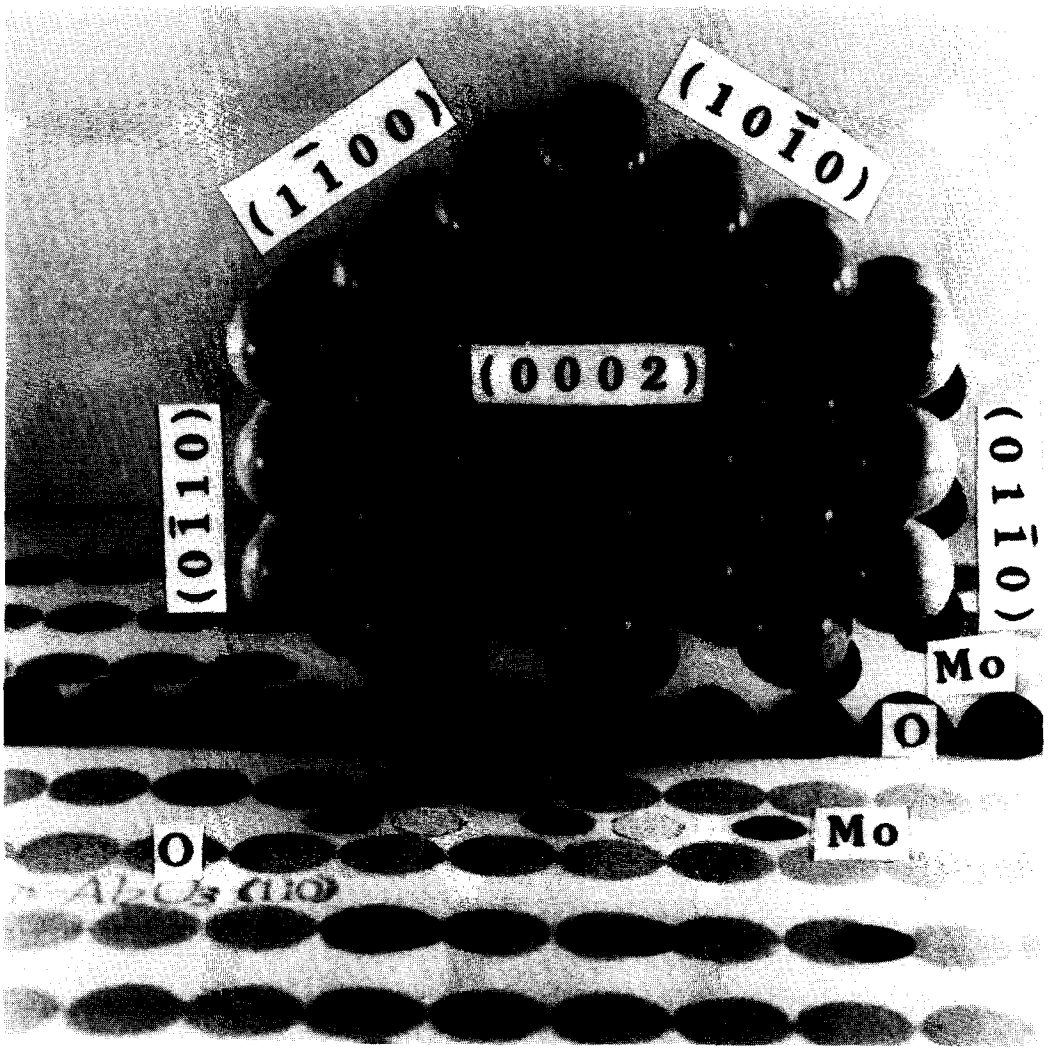

FIG. 9. Model of a MoS_2 crystallite bonded via the (2$\bar{1}\bar{1}$0) edge plane to the (110) γ-Al_2O_3.

through an Al–O–Mo linkage that leaves the stacking of the MoS_2 layers perpendicular to the Al_2O_3 (110) surface. The molybdenums in the remaining alternate slabs are not bonded to Al_2O_3 and fit directly between and above the oxygen rows in the (110) support surface. The slabs containing these latter molybdenums would then be held by van der Waals bonding to the other slabs.

As compared to the MoS_2 (2$\bar{1}\bar{1}$0) edge sets of planes, the bonding between the MoS_2 (10$\bar{1}$0) edge set of planes and the Al_2O_3 (110) surface is not nearly as favorable because of the mismatch in the distance between the more tightly packed molybdenums in a slab and the O–O distance in the support surface. In addition, the geometrical fit between higher index planes of MoS_2 and Al_2O_3 (110) was not nearly as good as with (2$\bar{1}\bar{1}$0). Other workers (*41, 45, 46*) have similarly proposed atomic structures for the edge bonding of single slabs of WS_2 by their (2$\bar{1}\bar{1}$0) plane to SiO_4 polyhedron in WS_2/Al_2O_3 catalysts. The bonding scheme advanced by our results extends the evidence for these edge-bonded structures to alumina-supported catalysts

TABLE 4

Statistical Analysis of Particle Dimensions

Sulfiding temperature	Number of particles	Range of d_{major} values (nm)	d_{major} ±SD[a] (nm)	(d_{minor}/d_{major}) ±SD
770	100	3.5 to 20.4	11.3 (±3.1)	0.576 (±0.17)
	15	7.0 to 8.4	7.8	0.660 (±.18)
	25	9.2 to 11.3	10.2	0.575 (±.16)
	47	12.0 to 14.8	13.4	0.536 (±.14)
910	100	7.7 to 43.6	25.9 (±7.4)	0.577 (±0.22)
	11	12.7 to 15.5	14.1 (±0.9)	0.518 (±0.19)
	23	16.2 to 22.5	20.1 (±1.6)	0.478 (±0.18)
	11	23.2 to 26.0	24.8 (±0.8)	0.421 (±0.24)
	26	26.7 to 29.5	28.3 (±0.9)	0.627 (±0.23)
	14	30.2 to 33.0	31.4 (±0.8)	0.687 (±0.14)
	8	33.7 to 36.6	34.9 (±1.0)	0.698 (±0.17)

[a] Standard deviation.

and also allows for multislab structures to still be edge-bonded onto alumina.

The observation that the angles between the edges of the faceted MoS_2 particles were very close to 120° suggests that the basal planes of the particles were at small angles to and perhaps nearly lying on the support surface. The smaller particles with one round edge and a diffuse, straight edge observed after 770 K sulfiding (e.g., see feature at B, Fig. 4) as well as elongated particles observed at both 770 and 910 K may also be truncated hexagons, but because of their large angles of orientation with the support and their smaller sizes, the hexagonal shapes were more difficult to distinguish.

The particle sizes and shapes in the CTEM micrographs of the catalysts sulfided at 770 and 910 K were characterized by measuring the minor (d_{minor}) and the major (d_{major}) dimensions of 100 particles for each sulfiding temperature. The average value of d_{major} increased from 11.2 and 25.9 nm as the temperature increased from 770 to 910 K (see Table 4), indicating that sintering had taken place. The particles were grouped into subsets according to their values of d_{major}, and average values of the aspect ratio (d_{minor}/d_{major}) were found for each subset (see Table 4).

The average aspect ratios are plotted versus the particle size (d_{major}) in Fig. 10. All of the particles at 770 K and the smaller particles sulfided at 910 K fall on the same curve. There is a break in the curve occurring for the larger particles that had been sulfided at 910 K (at ca. 30 nm), and a constant value of the aspect ratios is ap-

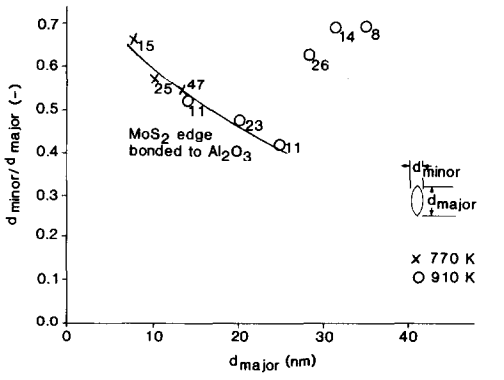

FIG. 10. Measured ratio of particle dimensions (d_{minor}/d_{major}) versus particle size after sulfiding at 770 and 910 K (the numbers beside each data point refer to the number of particles included in the average to give that point).

proached at large diameters. One explanation for the break in the curve is that the singularity occurs at the point where particles that have become oriented with their basal planes at right angles to the support become completely sulfided, the edge bonding to the support is broken, and the particles then become oriented parallel to the support. Indeed, the largest particles have hexagonal shapes with edges that have angles consistently equal to 120°, indicating that the MoS_2 basal plane is at small angles to and perhaps nearly lying on the support surface.

TEM studies of low-loading specimen: Reoxidation of sulfided samples. The 770 K-sulfided specimen with low Mo loading was reoxidized in O_2 for 100 ksec at 780 K and examined in CTEM. The bright field images after reoxidation are essentially the same as for the calcined sample, showing that the MoS_2 crystallites had wet and spread over the support during reoxidation. The above reoxidized sample was subsequently subjected to another sulfiding and oxidation treatment cycle, and the results were seen to be reversible. Specifically, sulfiding led to particle formation and reoxidation resulted in the disappearance of particles in the bright field CTEM micrographs. Evidently, the alumina support, because it is an oxide, has a stronger interaction with the Mo oxide rather than the Mo sulfide species. In contrast to Mo species which become sulfided, γ-Al_2O_3 has been observed to maintain its bulk oxide structure after sulfiding treatments as determined from gravimetric results (*47*).

The reversible nature of MoS_2/γ-Al_2O_3 catalysts with respect to sulfiding and oxidizing cycles has been observed for powdered catalysts of high surface area using other characterization techniques besides electron microscopy. These include studies by diffuse reflectance spectroscopy (*48–50*), infrared spectroscopy (*50*), XPS (*48–50*), and thermogravimetry (*48, 49*). These results offer evidence that low-surface-area, model catalysts provide useful representations of high-surface-area, powdered catalysts.

DISCUSSION

The Oxide Form of Mo/Al_2O_3

The results of the thin film catalysts in the oxide and sulfide forms and after oxidation confirm previous results by others obtained from high-surface-area catalysts and give additional insights about Mo/Al_2O_3 microstructure. In the oxide form, all Mo was present in a 6+ oxidation state, and there was a change in Mo oxide structure from a highly dispersed structure to a three-dimensional morphology as the Mo loading was increased. The change was evidenced both by the presence of orthorhombic MoO_3 particles in the bright field micrographs and by a decrease in Mo dispersion upon calcination, as measured by XPS. The Mo loading for which the change in structure took place was consistent with the filling of a monolayer of Mo oxide species observed by others (*36, 37, 51*) on high-surface-area catalysts (ca. 0.17 to 0.25 nm^2 Mo $atom^{-1}$).

Evidently, the highly dispersed nature of the Mo oxide phase on alumina is independent of the preparation method, whether it is by solution impregnation of polymolybdate anions (the usual method) or adsorption of $MoO_2(OH)_2$ (*36*) onto alumina powders, or, in this study, by thermal evaporation of MoO_3 onto thin films of alumina. In the solution impregnation method, polymolybdate anions of various sizes ($Mo_8O_{26}^{-4}$, $Mo_7O_{24}^{-6}$, MoO_4^{-2}) are formed depending on the pH of the solution and they bond onto Al_2O_3 sites forming strong Al–O–Mo linkages during drying and calcination (*52–55*). In the thermal evaporation of MoO_3 in vacuum (the method used in this study), molybdenum trioxide is known to be evaporated not as a monomer but as a polymer composed of three to five molecules (*56–58*).

In this study, highly dispersed Mo oxide was evidenced by a significant Mo signal in EDX that occurred in regions of the cata-

lyst that appeared to be featureless. This structure was present both in the catalyst with submonolayer loading and between the three-dimensional MoO_3 particles in the catalysts with greater than a monolayer loading. The highly dispersed structures may have been bonded to the alumina surface as a complete (*9, 10*) or incomplete monolayer (e.g., a chain structure (*47, 59*)) or they may have been bonded to alumina in small Mo oxide patches or clusters (*60, 61*).

The Sulfide Form of Mo/Al_2O_3

In this study, sulfiding led to the breakup of large, bulky MoO_3 crystallites and to the conversion of the highly dispersed oxide layer into MoS_2 crystallites. At normal sulfiding temperatures of ca. 670 K, highly dispersed oxide regions (of the intermediate loading specimen), which were believed to contain a full "monolayer" of Mo oxide species, were converted to 1- to 2-nm MoS_2 particles. High-resolution electron microscopy studies of conventional, high-surface-area supported catalysts have also observed the presence of 1- to 2-nm MoS_2 crystallites at a sulfiding temperature of 670 K. In these studies, lattice imaging of the 0.613-nm characteristic (0002) spacing between MoS_2 basal planes has resulted in the observation of curved and twisted sets of lines or threads in the bright field images (*62, 63*). The features have been observed more clearly on high-surface-area catalysts with larger MoS_2 crystallites, such as those present in unsupported catalysts (*64–69*) or in supported catalysts, in which sintering had taken place (*13, 64–66, 70, 71*). Recently, in two investigations, small particles in the same 1- to 2-nm size range have also observed after sulfiding at 673 K (*12, 72*). Zaikovskii *et al.* (*70*) have also observed 2- to 3-nm single-slab WS_2 crystallites in unpromoted and nickel-promoted W/SiO_2 catalysts prepared from impregnation of organometallic molecules.

At higher sulfiding temperatures (770 K), the average size of the crystallites was found in the present study to increase, as was found by other TEM studies (*12, 13*). Also, there remained a large number of small crystallites in the background along with the sintered crystallites, which was noticed by others on W/SiO_2 catalysts (*70*). After 770 K or higher temperature sulfiding of the sample with low molybdenum loading, the present study found that the MoS_2 crystallites were bonded via their edge planes to the alumina surface. Unlike other TEM studies which employed high-surface-area catalysts which had alumina crystallite surfaces oriented at all angles with respect to the electron beam, the present study used an alumina surface that was oriented predominantly in one direction with respect to the electron beam. Microdiffraction analysis of the 770 K-sulfided sample showed that many MoS_2 crystallites were oriented with their basal planes at large angles to the alumina surface. In addition, CTEM bright field images of the 910 K-sulfided sample showed the presence of MoS_2 hexagons that had been inhibited in growth along one dimension, giving them a truncated edge plane, perhaps indicating that they were (or had been) bonded along this plane to the support.

Both hypotheses of basal plane and edge plane bonding have been advanced in the literature. Early models assumed interaction of molybdenum sulfide species with alumina similar to the oxide form of the catalyst. Massoth (*47*) proposed an epitaxial chain model for both the oxide and sulfide forms of the catalyst, in which oxygen anions in the oxide form would be bonded less densely than a complete monolayer. Upon sulfiding, oxygen anions could be replaced by larger sulfur anions without destruction of the epitaxial morphology. Delannay (*62*) has recently postulated the existence of basal plane bonding, because some sets of MoS_2 lines in high-resolution electron microscopy lattice images appeared to wrap around the edges of alumina crystallites. On the other hand, Carver and Goetsch

(*73*) and Zaikovskii *et al.* (*70*) have postulated that the edge-up configuration dominates. Kochubei *et al.* (*46*) have recently proposed structural models for WS_2 on SiO_2 that included both edge bonding (with one slab of MoS_2 per crystallite) and basal bonding. They preferred edge bonding because the average coordination number of tungsten atoms (determined by EXAFS) increased slightly with the length of the slabs, in agreement with the behavior predicted by the model edge plane bonded structure and in contrast to the basal plane bonded structure. Hall has also discussed recently the probable presence of MoS_2 slabs edge bonded to alumina (*74*).

The manner of bonding, whether basal plane or edge plane, may affect catalytic activity. Topsøe *et al.* (*13, 16*) have noted an increase of two to three times in the specific activity for HDS as the sulfiding temperature was increased beyond a transition temperature that coincided with the appearance of free alumina hydroxyl bands in IR spectroscopy (*13, 45*). This so-called Type I-to-Type II transition (*13*) may correspond to a change in structure of MoS_2 from a basal plane bonded structure (the Type I catalyst) to an edge plane bonded structure (the Type II catalyst).

The present study confirms that the structural interaction between MoS_2 crystallites and the Al_2O_3 support in MoS_2/Al_2O_3 decreases as the sulfiding temperature is raised, which may be attributed to the breaking of Al–O–Mo linkages. CTEM bright field imaging and microdiffraction evidence show that basal planes of the MoS_2 crystallites are oriented at large angles with respect to the alumina surface as the particles grow at high sulfiding temperatures. At 670 K, sulfiding of the oxide form of the catalyst converts the oxygen anions not connected to the support (e.g., oxygens terminally bound to Mo or bridging between molybdenums) to sulfur anions, leaving the stronger Al–O–Mo linkages that are believed to be more resistant to sulfiding (*75*) intact.

Higher sulfiding temperatures cause an increasing fraction of Mo–O–Al linkages to become sulfided so that the basal planes of the MoS_2 crystallite may assume an orientation closer to the configuration of 90° with respect to the support. This behavior may be understood if Mo–O–Al linkages at the edges of the MoS_2 crystallites are stronger than those linkages on the basal plane of MoS_2; and, the latter linkages are thus sulfided before the Mo–O–Al linkages at the edge planes.

Finally, at higher sulfiding temperatures and with larger particles (ca. 30 nm), enough Mo–O–Al linkages become broken along the edge plane bonded to alumina so as to cause the crystallites oriented with their basal planes at 90° to the support to become oriented parallel to the support. In this state, these crystallites have little or no interaction with the support and are stabilized by weak van der Waals forces between their basal planes and the alumina surface.

From this study, identification of so-called Type I catalysts is made with MoS_2 crystallites that have small angles of orientation of their basal planes with the support. The cause of the lower specific HDS activity of Type I sites may be a result of a sterically hindered environment of the edge plane active sites adjacent to the support as adsorption and/or reaction sites for large aromatic sulfur reactants. The Type II catalysts are identified with MoS_2 crystallites that have angles of orientation closer to 90° with the support, and these Type II catalysts would have MoS_2 edge sites with no steric hindrance for bulky sulfur compounds. We also suggest that Type II′ catalysts exist for which the edge bonding of MoS_2 to alumina has been broken by extensive sulfiding and the crystallites are oriented with their basal planes parallel to the support surface. These catalysts would have HDS activities similar to Type II catalysts, since Type II′ MoS_2 crystallites have a large dimension along their *c* axes; thus most edge sites would not be in close proximity to the alumina surface and little steric

hindrance for reactant molecules would exist.

Finally, the electron micrographs of the present study give evidence for faceted MoS_2 single crystals, and this confirms the existence of specific edge plane and corner sites. The present study also found that the MoS_2 crystallites were shaped as hexagons with a truncated edge bonded to the alumina support. The edge planes in contact with the gas phase were assigned to the $(10\bar{1}0)$ set of MoS_2 crystal planes and the truncated edge plane bonded to the support was assigned to the $(2\bar{1}\bar{1}0)$ set of planes. The assignment was based on the measured angle between the truncated and catalytically active edges in the bright field images, the surface energy estimate for $(10\bar{1}0)$ being lower than that for $(2\bar{1}\bar{1}0)$, and the excellent geometrical fit of the (2110) bonding plane to the most stable (110) γ-Al_2O_3 surface plane.

CONCLUSIONS

Consistent with findings on high-surface-area powders, Mo oxide species present in alumina-supported, model thin-film catalysts after calcination were highly dispersed and thus not visible in transmission electron micrographs for loadings below ca. 5 Mo atoms nm^{-2}. Above this loading, some Mo species were highly dispersed and others were present as orthorhombic MoO_3 crystallites, the latter of which were discernible in the bright field micrographs. Sulfiding in 6% H_2S/H_2 led to the destruction of the MoO_3 crystallites and the highly dispersed Mo oxide at 670 to 770 K, with the formation of MoS_2 crystallites. The MoS_2 crystallites were present as thin, hexagonally shaped slabs with one truncated edge. These crystallites were bonded with their high-energy edge planes to the support surface. The edge planes contacting the gas phase, and presumably active in catalytic reactions, were assigned as the $(10\bar{1}0)$ set of planes, while the truncated edge bonded to the surface of alumina was assigned as the $(2\bar{1}\bar{1}0)$ plane. Reoxidation produced a reversible spreading of Mo species onto the alumina support.

It is proposed that the highly dispersed oxide form of the catalyst is composed of Mo oxide species present as small clusters. These clusters are anchored to the support through Mo–O–Al linkages having a distribution of strengths. Sulfiding at successively higher temperatures results in breaking more of these linkages, thereby causing the MoS_2 basal planes to become oriented perpendicular to the support surface due to favorable bonding between the MoS_2 edge planes and the support. The MoS_2 crystallites eventually became oriented with their basal planes parallel to the support when the Mo–O–Al linkages at the edge planes are finally broken (at temperatures near 910 K). The higher specific activity for thiophene HDS of structures formed after high sulfiding temperatures (Type II structures) can be explained by less steric hindrance of bulky sulfur-containing aromatics in reaching the edge plane active sites for adsorption that are not in close proximity to the support surface.

ACKNOWLEDGMENTS

We wish to acknowledge the donors of the Petroleum Research Fund, administered by the American Chemical Society, for the partial support of this research. We also acknowledge stimulating discussions with Henrik Topsøe, Øle Sorensen, and Bjerne Clausen of the Haldor Topsøe Research Laboratories.

REFERENCES

1. Lombardo, E. A., LoJacano, M., and Hall, W. K., *J. Catal.* **64,** 150 (1980).
2. Gates, B. C., Katzer, J. R., and Schuit, G. C. A., "Chemistry of Catalytic Processes." McGraw-Hill, New York, 1979.
3. Massoth, F. E., "Advances in Catalysis," Vol. 27, p. 265. Academic Press, New York, 1978.
4. Grange, P., *Catal. Rev.-Sci. Eng.* **21,** 135 (1980).
5. Topsøe, H., and Clausen, B. S., *Catal. Rev.-Sci. Eng.* **26,** 395 (1984).
6. Berispek, V., M.S. thesis. Virginia Polytechnic Institute and State University, Blacksburg, Virginia, 1975.
7. Newsome, D. S., *Catal. Rev.-Sci. Eng.* **21,** 275 (1980).

8. Topsøe, H., Candia, R., Topsøe, N.-Y., and Clausen, B. S., *Bull. Soc. Chim. Belg.* **93,** 783 (1984).
9. Schuit, G. C. A., and Gates, B. C., *AIChE J.* **14,** 159 (1968).
10. Schuit, G. C. A., and Gates, B. C., *AIChE J.* **19,** 417 (1973).
11. Delannay, F., *Catal. Rev.-Sci. Eng.* **22,** 141 (1980).
12. Prada Silvy, R., Beuken, J. M., Bertrand, P., Hodnett, B. K., Delannay, F., and Delmon, B., *Bull. Soc. Chim. Belg.* **93,** 775 (1984).
13. Candia, R., Sørensen, O., Villadsen, J., Topsøe, N.-Y., Clausen, B. S., and Topsøe, H., *Bull. Soc. Chim. Belg.* **93,** 763 (1984).
14. Tauster, S. J., Pecoraro, T. A., and Chianelli, R. R., *J. Catal.* **63,** 515 (1983).
15. Voorhoeve, R. J. H., and Stuiver, J. C. M., *J. Catal.* **23,** 243 (1971).
16. Candia, R., Topsøe, H., and Clausen, B. S., *in* "Proceedings, 9th Iberoamerican Symposium on Catalysis," p. 211. Lisbon, Portugal, 1984.
17. Topsøe, H., Clausen, B. S., Topsøe, N.-Y., and Pedersen, E., *Ind. Eng. Chem.*, in press.
18. Massoth, F. E., Muralidhar, G., and Shabtai, J., *J. Catal.* **85,** 53 (1984).
19. Hayden, T. F., Ph.D. dissertation. University of Wisconsin–Madison, 1986.
20. Ruckenstein, E., and Malhotra, M. L., *J. Catal.* **41,** 303 (1976).
21. Ruckenstein, E., and Chen, J. J., *J. Catal.* **70,** 233 (1981).
22. Chu, Y. F., and Ruckenstein, E., *J. Catal.* **55,** 281 (1978).
23. Chen, J. J., and Ruckenstein, E., *J. Phys. Chem.* **85,** 1606 (1981).
24. Varon, J., Schiaro, J., and Janus, T. P., *Rev. Sci. Instrum.* **38,** 691 (1967).
25. Glassl, H., Kramer, R., and Hayek, K., *J. Catal.* **63,** 164 (1980).
26. Stulga, J. E., Wynblatt, P., and Tien, J. K., *J. Catal.* **62,** 59 (1980).
27. Diggle, J. W., Downie, T. C., and Goulding, C. W., *Chem. Rev.* **69,** 365 (1969).
28. Van Cittert, P. H., *Z. Phys.* **69,** 298 (1931).
29. Burger, H. C., and Van Cittert, P. H., *Z. Phys.* **79,** 722 (1932).
30. Madden, H. H., and Houston, J. E., *J. Appl. Phys.* **47,** 3071 (1976).
31. Madden, H. H., and Houston, J. E., *Adv. X-Ray Anal.* **19,** 657 (1976).
32. Krause, M. O., and Fereira, J. B., *J. Phys.* **8,** 2007 (1975); *J. Phys. Chem. Ref. Data* **8,** 329 (1979).
33. Davis, G. D., Viljoen, P. E., and Lagally, M. G., *J. Electron Spectrosc. Relat. Phenom.* **21,** 135 (1980).
34. Matthew, J. A. D., and Underhill, P. R., *J. Electron Spectrosc. Relat. Phenom.* **14,** 371 (1978).
35. Fadley, C. S., *in* "Electron Spectroscopy: Theory, Techniques, and Applications" (C. R. Brundle and A. D. Baker, Eds.), Vol. II, p. 1. Academic Press, New York/London, 1978.
36. Sonnemans, S., and Mars, P., *J. Catal.* **31,** 209 (1973).
37. Zingg, D. S., Makovsky, L. E., Tischer, R. E., Brown, F. R., and Hercules, D. M., *J. Phys. Chem.* **84,** 2898 (1980).
38. Patterson, T. A., Carver, J. C., Leyden, D. E., and Hercules, D. M., *J. Phys. Chem.* **80,** 1700 (1976).
39. Treacy, M. M. J., Howie, A., and Wilson, C. J., *Philos. Mag., [Part] A* **38,** 569 (1978).
40. Wyckoff, R. W. G., "Crystal Structures," Vols. 1 and 2. Wiley, New York, 1963.
41. Yermakov, Yu. I., Startsev, A. N., Burmistrov, V. A., Shumilo, O. N., and Bulgakov, N. N., *Appl. Catal.* **18,** 33 (1985).
42. Farragher, A. L., *Adv. Colloid Interface Sci.* **11,** 3 (1979).
43. Farragher, A. L., "The Role of Solid State Chemistry in Catalysis." Amer. Chem. Soc., Div. Petr. Chem., Washington, D.C., 1977.
44. Lippens, B. C., Ph.D. thesis. Technical University of Delft, The Netherlands, 1961.
45. Moroz, E. M., Bogdanov, S. V., Tsybulya, S. V., Burmistrov, V. A., Startsev, A. N., and Yermakov, Yu. I., *Appl. Catal.* **11,** 173 (1984).
46. Kochubei, D. I., Kozlov, M. A., Zamaraev, K. I., Burmistrov, V. A., Startsev, A. N., and Yermakov, Yu. I., *Appl. Catal.*, in press.
47. Massoth, F. E., *J. Catal.* **36,** 164 (1975).
48. Chung, K. S., and Massoth, F. E., *J. Catal.* **64,** 320 (1980).
49. Chung, K. S., and Massoth, F. E., *J. Catal.* **64,** 332 (1980).
50. Massoth, F. E., *J. Catal.* **54,** 450 (1978).
51. Dufresne, P., Payen, E., Grimblot, J., and Bonnelle, J. P., *J. Phys. Chem.* **85,** 2344 (1981).
52. Wang, L., and Hall, W. K., *J. Catal.* **77,** 232 (1982).
53. Dufaux, M., Che, M., and Naccache, C., *J. Chim. Phys.* **67,** 527 (1970).
54. Hall, W. K., and Massoth, F. E., *J. Catal.* **34,** 41 (1974).
55. Millman, W. S., Crespin, M., Cirillo, Jr., A. C., Abdo, S., and Hall, W. K., *J. Catal.* **60,** 404 (1979).
56. Blackburn, P. E., Hoch, M., and Johnston, H. L., *J. Phys. Chem.* **62,** 764 (1938).
57. Dushman, S., "Scientific Foundations of Vacuum Technique," p. 760. Wiley, New York, 1962.
58. Maissel, I., and Glang, R., "The Handbook of Thin Film Technology." McGraw–Hill, New York, 1970.
59. Massoth, F. E., *J. Less-Common Met.* **54,** 343 (1977).

60. Hall, W. K., *in* "Proceedings, 4th International Conference on the Chemistry and Uses of Molybdenum." Golden, Colorado, 1982.
61. Cirillo, A. C., Dollish, F. R., and Hall, W. K., *J. Catal.* **62,** 379 (1980).
62. Delannay, F., *Appl. Catal.* **16,** 135 (1985).
63. Hirsch, P. B., Howie, A., Nicholson, R. B., Pashley, D. W., and Whelan, M. J., "Electron Microscopy of Thin Crystals." Butterworths, Washington, D.C., 1965.
64. Sanders, J. V., *Chem. Scr.* **14,** 141 (1978).
65. DeBeer, V. H. J., and Schuit, G. C. A., *in* "Preparation of Catalysts" (B. Delmon, P. A. Jacobs, and G. Poncelet, Eds.), p. 343. Elsevier, Amsterdam, 1976.
66. Sanders, J. V., and Pratt, K. C., *J. Catal.* **67,** 331 (1981).
67. Sørensen, O., Clausen, B. S., Candia, R., and Topsøe, H., *Appl. Catal.* **13,** 363 (1985).
68. Candia, R., Clausen, B. S., and Topsøe, H., *Bull. Soc. Chim. Belg.* **90,** 1225 (1981).
69. Delannay, F., Thakur, D. S., and Delmon, B., *J. Less-Common Met.* **63,** 265 (1979).
70. Zaikovskii, V. I., Plyasova, L. M., Burmistrov, V. A., Startsev, A. N., and Yermakov, Yu. I., *Appl. Catal.* **11,** 15 (1984).
71. Pratt, K. C., and Sanders, J. V., *in* "Proceedings, 7th International Congress on Catalysis, Tokyo, 1980" (T. Seiyama and K. Tanabe, Eds.), p. 1420. Kodansha, Ltd., Tokyo, 1981.
72. Prada, R., Delannay, F., and Delmon, B., to be published.
73. Carver, J. C., and Goetsch, D. A., 186th ACS National Meeting, Abstract Coll. 92.
74. Hall, W. K., *in* "Chemistry and Physics of Solid Surfaces" (R. Vanselow and R. S. Howe, Eds.), Vol. VI. Springer-Verlag, in press.
75. Schrader, G. L., and Cheng, C. P., *J. Catal.* **80,** 369 (1983).